Available online at www.sciencedirect.com
ScienceDirect
Trans. Nonferrous Met. Soc. China 33(2023) 2483−2496
Transactions of Nonferrous Metals Society of China
www.tnmsc.cn

Structure and tribological properties of $MoSe_2$ films prepared by two-step process

Wen-yi ZHAN, Jian-peng ZOU, Xu MAO, Lei TANG, Hong-ming WEI

State Key Laboratory of Powder Metallurgy, Central South University, Changsha 410083, China

Received 3 March 2022; accepted 27 May 2022

Abstract: In order to extend the application range of solid lubricant $MoSe_2$, a two-step process was adopted to prepare the $MoSe_2$ film. Namely, the $MoSe_x$ precursor layer was firstly deposited on the substrate by magnetron sputtering method, and then selenized in a Se vapor atmosphere to obtain $MoSe_2$ film. The effects of the sputtering and selenization process on the structure and tribological properties of the films were investigated. The results show that the two-step prepared $MoSe_2$ films exhibit a preferential orientation with (002) basal plane parallel to the substrate and an improved crystallinity. The prepared $MoSe_2$ film has good wear resistance and lubricating performance in an ambient air environment, with the lowest average friction coefficient of 0.0443 and a specific wear rate of 1.03×10^{-5} $mm^3/(N\cdot m)$. In addition, the lubrication effects of $MoSe_2$ films through the adhesion mechanism and fill in-repair mechanism were further discussed.

Key words: $MoSe_2$ film; magnetron sputtering; selenization; tribological property; lubrication mechanism; 3D profile

1 Introduction

The graphene-like layered transitional metal dichalcogenides (TMDCs) can usually be denoted as the formula MX_2, where M is transitional metal elements (including W, Mo, Ti, V, etc.) and X stands for chalcogen (S, Se, Te, etc.) [1]. The existence of weak van der Waals force between layers of TMDCs makes the interlayer slip appear easily, which can play an important role in anti-friction and lubrication [2]. Numerous researchers have studied the lubrication effects of TMDCs since the last century, such as MoS_2 and WS_2. However, the low-friction MoS_2 deteriorates in humid air and high temperature, which restricts the development and application of MoS_2 lubricant under terrestrial conditions on earth [3]. Remarkably, selenides, such as $MoSe_2$ and WSe_2, show better temperature stability and lower sensitivity to the humid atmosphere than similar sulfides [3,4]. For example, LI et al [5] investigated the tribological properties of hydrothermally synthesized $MoSe_2$ nanoparticles as white oil additives. They found that the smaller size of $MoSe_2$ nanoparticles dispersed in oil could achieve a lower friction coefficient and wear rate, which was inferred to be conducive to the formation of the transfer film during friction. Furthermore, KUBART et al [3] investigated the tribological performance of $MoSe_2$ films prepared by magnetron sputtering and found the formation of protective films on the friction-test counterpart balls. However, the lubrication mechanism of pure $MoSe_2$ anti-friction film remains unclear. Therefore, it is of great significance to investigate the lubrication mechanism which would be an instruction for the industrial practical applications of solid lubricant coatings.

Various coating techniques have been developed to fabricate films, such as CVD [6], sol−gel method [7], magnetron sputtering [8,9], and

Corresponding author: Jian-peng ZOU, Tel: +86-731-88876630, E-mail: zoujp@csu.edu.cn
DOI: 10.1016/S1003-6326(23)66275-2

ALD [10]. Compared with other methods, magnetron sputtering is suitable for large areas and homogeneous film production and its cost is relatively low, so it has been applied in industrial manufacturing widely. There are various studies that focus on preparing $MoSe_2$ films through magnetron sputtering [11,12]. However, it is well known that the pure sputtered $MoSe_2$ film normally exhibited a porous columnar microstructure [13], which limits the tribological performance of the lubricating film. Also, some researchers tried to use the magnetron sputtering to deposit a Mo film on the substrate and selenize the Mo film under selenium vapor to gain the $MoSe_2$ film [14,15]. By comparison, this traditional selenization approach of transforming Mo into $MoSe_2$ film could obtain higher compactness [16]. Nevertheless, the interface bonding performance would be relatively poor through traditional selenization of sputtered Mo film due to the large expansion from Mo to $MoSe_2$ with different densities (ρ_{Mo}=10.2 g/cm^3, and ρ_{MoSe_2}=6.0 g/cm^3) [17]. To improve the interface adhesion and reduce the expansion, we proposed the preparation procedure of $MoSe_2$ films through a two-step method, combining the radio frequency (RF) magnetron sputtering of a $MoSe_2$ target and the following selenization of the sputtered $MoSe_x$ precursor film into $MoSe_2$ film, which would provide guidance for industrial production and application of high-quality $MoSe_2$ lubricant coatings. It is expected to improve the porous microstructure of pure sputtered $MoSe_2$ film and reduce the expansion by selenizing the $MoSe_x$ precursor film rather than Mo film.

In this work, $MoSe_2$ films with high (002) orientation were successfully prepared on the substrates by a two-step method combing RF magnetron sputtering and subsequent selenization. The effects of the two-step procedure on the structures and compositions of the prepared films were studied. The influence of the sputtering and the selenization parameters on the tribological properties of $MoSe_2$ films was systematically researched. And the anti-friction mechanisms of $MoSe_2$ films grown on stainless steel substrates were further proposed and discussed.

2 Experimental

2.1 Experimental process

$MoSe_2$ films were prepared using a two-step method, namely, the $MoSe_x$ precursor layer was firstly deposited on the substrate by RF magnetron sputtering with a $MoSe_2$ target (99.99% purity, and diameter of 60 mm, ZhongNuo Advanced Material Technology Co., Ltd., China), and then selenized in a Se vapor atmosphere to obtain $MoSe_2$ film. The films prepared on quartz glass substrates (20 mm × 10 mm × 1 mm) were selected for the analysis of composition, structure and morphology, and those on polished 304 stainless steel substrates (d25 mm × 4 mm) were applied for the analysis of tribological properties. The quartz glass and steel substrates were ultrasonically cleaned in acetone, ethanol, and distilled water for 15 min, respectively. The cleaned substrates were preserved in ethanol and dried with N_2 before putting into the magnetron sputtering system (JGP−450, Sky Technology Development Co., Ltd.). The sputtering chamber was evacuated to a background below 8×10^{-4} Pa. The $MoSe_x$ precursor films prepared on quartz substrates were deposited at Ar pressure of 0.2 Pa for 30 min at various powers (30, 60, 90, and 120 W), and the substrate holder was rotated to ensure the uniformity of the films. Pre-sputtering for 10 min was employed to clean the surface of the target before deposition. The deposition was carried out at room temperature and the substrate temperature was not controlled. Afterward, $MoSe_x$ precursor films were selenized with sufficient Se powder in a tubular sliding furnace with two heating areas (OTF−1200X−50−SL, Hefei Kejing Materials Technology Co., Ltd., China). Before the selenization, the quartz tube was pumped to 0.8 Pa and filled with N_2 to 1.013×10^5 Pa, and this process was repeated three times to exhaust residual oxygen. The furnace was heated on one side to the required selenization temperature with a heating rate of 10 °C/s, and then slid to the sample area for selenization. $MoSe_2$ films on quartz substrates were acquired after selenizing for 30 min at 500 °C and cooling naturally to room temperature. The deposition and selenization parameters for $MoSe_2$ films prepared on 304 steel substrates were discussed and optimized in the later section of the tribological properties investigation.

2.2 Characterization method

The crystal structures were characterized by an X-ray diffractometer (XRD, D/max 2550VB, Rigaku Ltd.) using Cu K_α radiation (λ=1.5406 Å) at

a voltage of U=30 kV and current of I=200 mA in the 2θ range from 10° to 80°. And Raman spectroscopy (LabRAM HR800, HORIBA Jobin Yvon) observation was performed with 532 nm laser excitation. The surface and cross-section morphologies of $MoSe_2$ films were obtained by scanning electron microscopy (SEM, Helios Nanolab G3 UC, FEI). Energy dispersive spectrometer (EDS, Aztec Energy X-max 80, Oxford Instruments Ltd.) was used to get the element distribution on the cross-section of the film. The chemical composition and valence analyses of the films were carried out by X-ray photoelectron spectroscopy (XPS, ESCALAB250Xi, Thermo-Fisher-VG Scientific) using the monochromatic Al K_α X-ray source (1486.7 eV). The quantitative studies were based on the determination of the Mo 3d and Se 3d peak area with 9.5 and 2.29 as sensitivity factors (the sensitivity factors of the spectrometer are given by the manufacturer), respectively. The tribological tests of $MoSe_2$ films were employed with a ball-on-disk tribometer (UMT−2MT, CETR Corporation Ltd., USA) under ambient conditions. The counterparts were the GCr15 balls (diameter of 6 mm) and the tests were conducted at a rotating speed of 100 r/min and a load of 2 N for 30 min. The diameter of the wear track was 12 mm. The wear scars on the tested samples were characterized by a non-contact optical three-dimensional profilometer (NanoMap-D, Aep Technology Inc., USA). Specific wear rates were calculated as worn volume per sliding distance and load after 3000 revolutions of the friction test. The wear tracks imaging was done using optical microscopy (M203−M50, AOSVI).

3 Results and discussion

3.1 Effect of sputtering power on $MoSe_2$ films

The $MoSe_x$ precursor films were sputtered onto the quartz substrates at sputtering powers of 30, 60, 90, and 120 W, respectively. The Raman spectra of the $MoSe_x$ precursors are shown in Fig. 1(a). The peaks at 244 and 283 cm^{-1} correspond to the out-of-plane A_{1g} and in-plane E^1_{2g} phonon modes of $MoSe_2$ [18]. Precursor film deposited at 30 W has an amorphous structure without a distinct characteristic peak, while A_{1g} and E^1_{2g} peaks appear at sputtering power higher than 30 W. It is supposed that the sputtering power will affect the kinetic

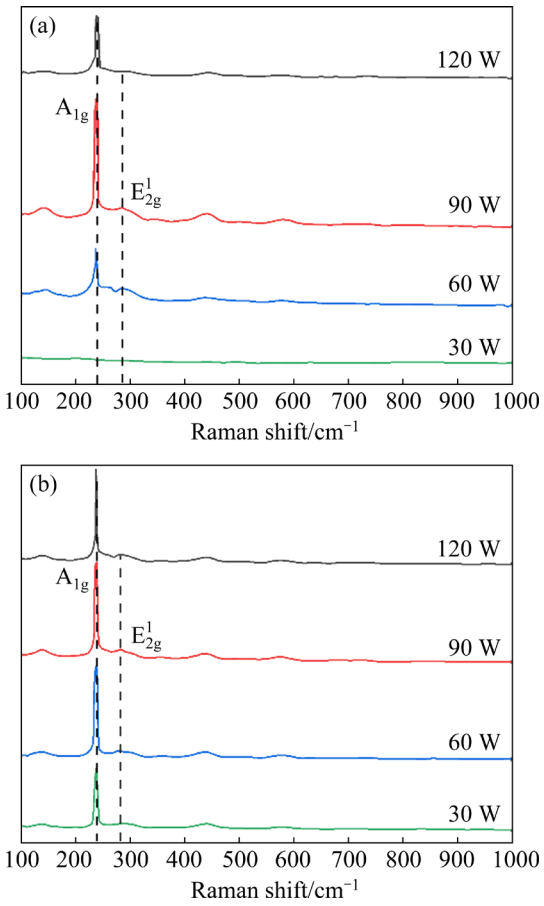

Fig. 1 Raman spectra of $MoSe_x$ films prepared at different sputtering powers (a) and corresponding selenized $MoSe_2$ films (b)

energy and yield of sputtered atoms during the deposition process and impact the growth and crystallization of film [14]. While low sputtering power (30 W) has insufficient energy of sputtered atoms to crystalize, and high sputtering power (120 W) with excessive energy of sputtered atoms will cause severe bombardment to the formed film (preferential re-sputtering), which is detrimental to the film. Figure 1(b) shows the Raman spectra of the $MoSe_2$ films obtained after the selenization of $MoSe_x$ precursor films. When the precursor film of 30 W was selenized, the A_{1g} peak of $MoSe_2$ appeared on the spectrum, indicating an improved crystallinity. For the samples prepared at 60 and 120 W in Fig. 1(b), the A_{1g} peaks are raised and the crystallinities are improved compared with those in Fig. 1(a).

Figures 2(a−c) present the XPS spectra of $MoSe_x$ precursor film prepared at the sputtering power of 60 W. The XPS wide scan and detailed

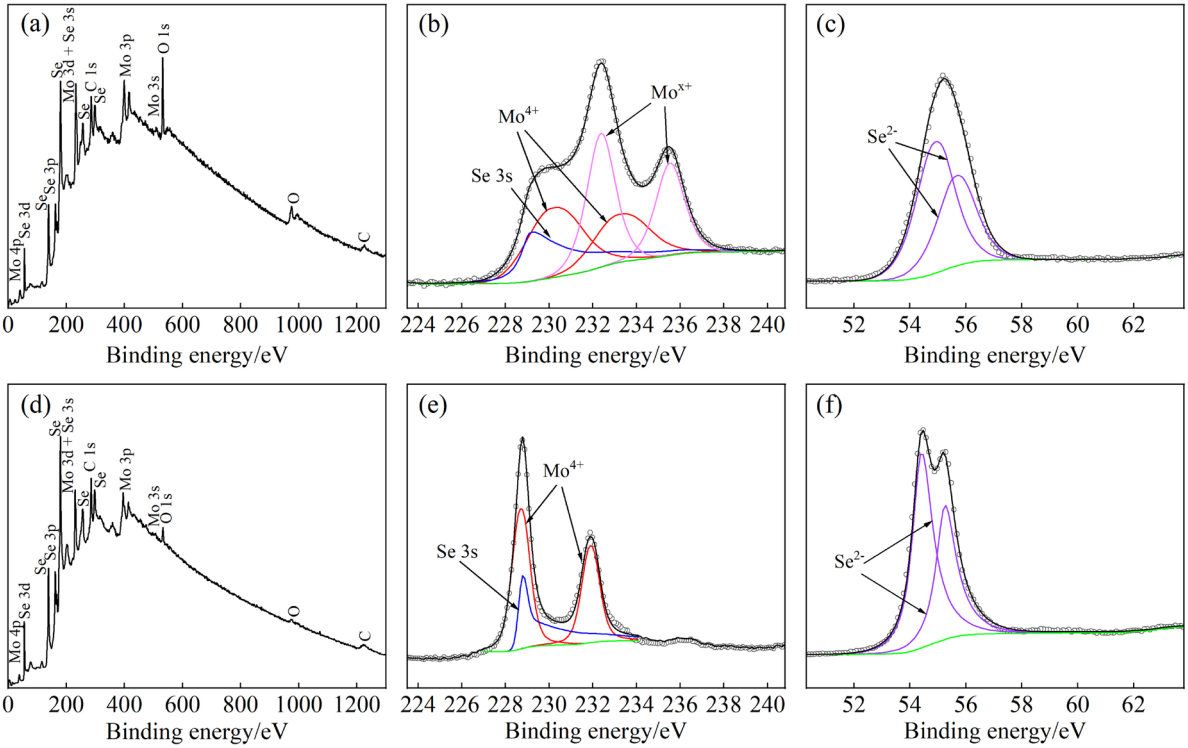

Fig. 2 XPS spectra of $MoSe_x$ film at sputtering power of 60 W (a−c) and $MoSe_2$ film selenized at 500 °C (d−f): (a, d) Survey spectra; (b, e) Mo 3d; (c, f) Se 3d

scans are calibrated with respect to the adventitious carbon peak at 284.8 eV. The survey spectrum shows the chemical composition on the surface of the precursor film which is labeled in Fig. 2(a). The narrow scans exhibited in Figs. 2(b, c) are fitted using the Lorentzian−Gaussian function to identify the chemical valence states of Mo and Se elements in the film. The fitted Mo $3d_{5/2}$ peaks located at 230.12 and 232.37 eV are presumed to arise from $MoSe_2$ (Mo^{4+}) and molybdenum oxide (Mo^{x+}, $x \geq 4$), respectively. While the binding energy of Se $3d_{5/2}$ located at 54.89 eV in Fig. 2(c) is supposed to be Se^{2-} from $MoSe_2$. The quantitative study shows the $MoSe_x$ precursor film is selenium-deficient with a Se/Mo molar ratio of 1.03. This may be due to different sputtering rates between Mo and Se atoms during the deposition, and thus the non-stoichiometric and amorphous $MoSe_x$ precursor film is formed. Figures 2(d−f) show the corresponding XPS spectra of the selenized $MoSe_2$ film. The survey spectrum shows that the oxidation on the surface of the $MoSe_2$ film is significantly reduced in Fig. 2(d), considering the inevitable contamination in the atmosphere. The binding energies for Mo 3d doublet of the selenized film at 500 °C are found to be 228.69 eV (Mo $3d_{5/2}$) and 231.88 eV (Mo $3d_{3/2}$) in Fig. 2(e), which are consistent with the literature [6]. And the doublet peaks of Se 3d are located at 54.46 eV (Se $3d_{5/2}$) and 55.33 eV (Se $3d_{3/2}$) in Fig. 2(f). The quantitative analysis shows a higher Se/Mo molar ratio of 1.72 after the selenization. The disappearance of molybdenum oxide (Mo^{x+}) peaks in Fig. 2(e) is consistent with the result in Fig. 2(d). These XPS spectra demonstrate that the selenization procedure can increase stoichiometry and improve the valence state composition of the film.

Figure 3 shows the XRD patterns of $MoSe_x$ precursor film sputtered at 60 W and selenized $MoSe_2$ films prepared at 30, 60, 90, and 120 W, respectively. The broad peak corresponding to SiO_2 from the quartz glass substrate is observed at 2θ=21.3°. The diffraction peaks at 2θ=13.77°, 27.56°, 42.06°, and 56.87° correspond to the (002), (004), (006), and (110) crystal planes of $MoSe_2$ (JCPDS No.29-0914), respectively. The XRD patterns of all selenized $MoSe_2$ films show the texture of (002) preferred orientation. When the sputtering power is 60 W, the corresponding $MoSe_2$ thin-film owns the highest intensity of the (002) characteristic peak and the better crystallinity. Combined with Fig. 1(a), the Raman spectrum of

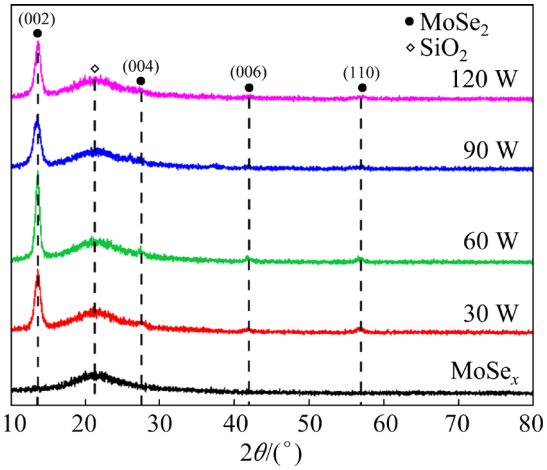

Fig. 3 XRD patterns of selenized $MoSe_2$ films prepared at different sputtering powers and $MoSe_x$ precursor film

the $MoSe_x$ prefabricated film obtained at the sputtering power of 90 W achieves the highest intensity of A_{1g} peak, which shows that the sample has a relatively low concentration of lattice defects, resulting in lower activity of selenization process. Therefore, the (002) peak of selenized $MoSe_2$ film at 90 W is lower than that of the $MoSe_2$ sample prepared at 60 W. Although the $MoSe_x$ precursor prepared at 30 W has a poor signal in Fig. 1(a), its crystallinity is significantly improved and has (002) preferential orientation after 30 min selenization in Fig. 3. However, the thickness of the $MoSe_x$ precursor film deposited on the glass substrate is thinner due to its lower sputtering power, accounting for the lower intensity of (002) peak of selenized film than the corresponding $MoSe_2$ film prepared at 60 W. The $MoSe_x$ precursor film prepared at the sputtering power of 60 W has both crystalline and amorphous characteristics, while the amorphous characteristic owns more lattice defects and higher diffusion activity, thus presenting a higher preference for (002) orientation and crystal integrity after selenization [19]. When the sputtering power is elevated to 120 W, the preferential re-sputtering with excessive energy of sputtered atoms will damage the inner layer. The crystallinity of the $MoSe_2$ film at 120 W is improved after the selenization, but is still lower than that of the sample prepared at 60 W.

Figure 4 shows the top-view SEM images of corresponding $MoSe_2$ films after selenization of the $MoSe_x$ precursor films prepared at different sputtering powers. These four films all have dense structures. And there are some convex structures on the surfaces of these four films, but the surface morphology does not change obviously with the increase of sputtering power.

To observe the cross-section morphology of the $MoSe_2$ film, the sputtering was extended to 80 min at 60 W to increase the thickness of the film, and the specimen was snapped with a diamond

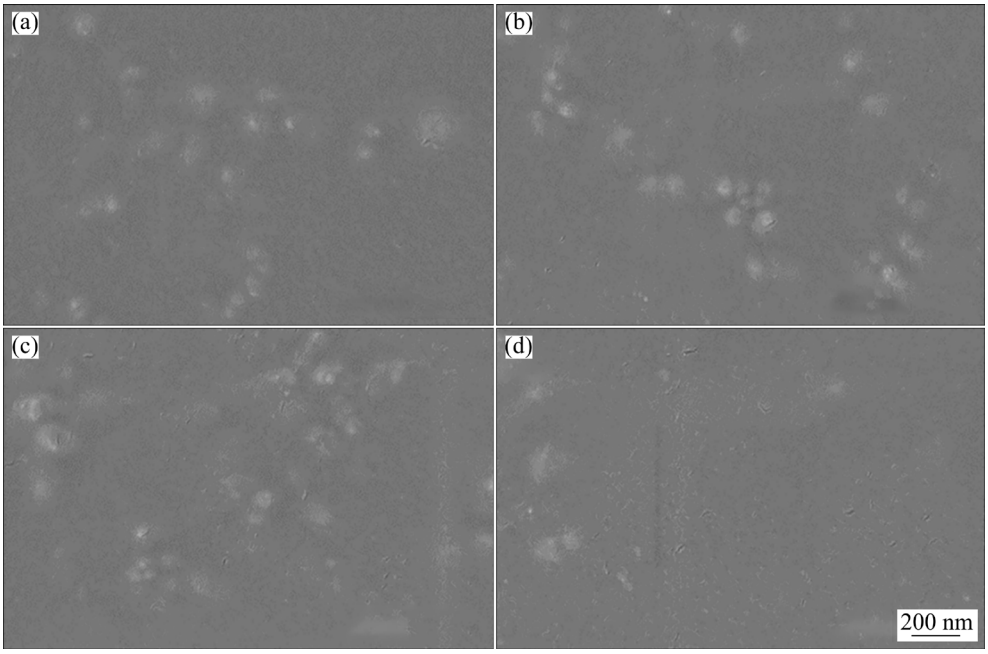

Fig. 4 SEM surface morphologies of selenized $MoSe_2$ films at different sputtering powers: (a) 30 W; (b) 60 W; (c) 90 W; (d) 120 W

cutter after the selenization for 30 min. There are two typical structures in Fig. 5(a), the outer layer of $MoSe_2$ film, and the inner layer of $MoSe_x$ precursor film which is incompletely selenized. The structure of the $MoSe_2$ film is compact without significant defects, while the inner $MoSe_x$ precursor film has a columnar microstructure with some pores. The total thickness of the film is about 3.0 μm. The chemical distribution of the cross-section film is characterized by the EDS linear scan shown in Fig. 5(b), which demonstrates that the composition of the outer layer $MoSe_2$ film is relatively uniform. However, the composition of the film begins to fluctuate at the distance of about 2.5 μm from surface to substrate, which is the result of the incompletely selenized $MoSe_x$ precursor film with a lower Se content. This is consistent with the XPS result in Fig. 2. During the selenization process, as the $MoSe_x$ precursor film further crystallizes, grows, expands, and densifies, it becomes more difficult for the Mo atoms to diffuse from the inner layer to the surface, so that the content of Mo on the surface is reduced. There is not sufficient content of Mo atoms to form $MoSe_2$, which results in a relatively low content of Se on the surface of the film. The slight rise of O content in the area between the precursor film and substrate is probably the consequence of the diffusion effect of SiO_2 glass at high temperature.

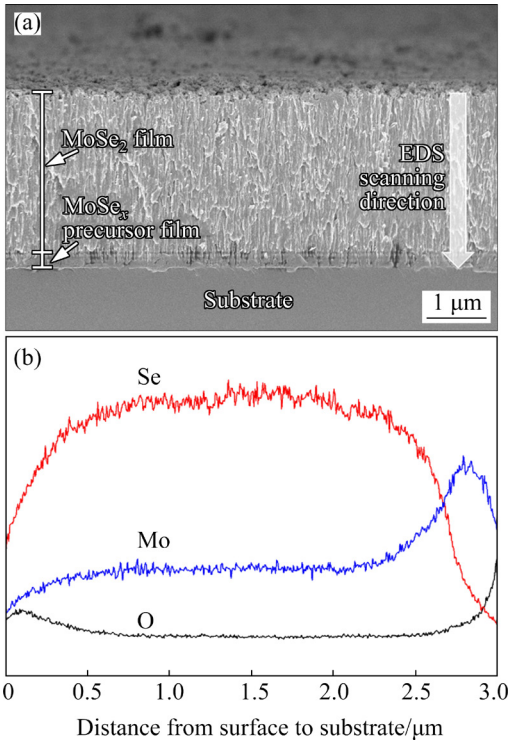

Fig. 5 Cross-sectional SEM morphology (a) and EDS linear scanning curves (b) of selenized $MoSe_2$ film

3.2 Tribological properties of $MoSe_2$ films

The 304 stainless steel was selected as the substrate in this section to investigate the tribological properties of $MoSe_2$ films. The following experiments were carried out at the sputtering power of 60 W. The tribological properties of the $MoSe_2$ films on 304 steel substrates prepared at various sputtering pressures, sputtering time, selenization temperatures, and selenization time were investigated and optimized, respectively. The friction coefficients of the films were calculated by a ball-on-disk tribometer, and a profilometer was used to depict the worn surface of the films.

3.2.1 Effect of sputtering pressure on tribological properties of $MoSe_2$ films

The $MoSe_x$ precursor films on 304 stainless steel substrates were prepared at different sputtering pressures of 0.2, 1.0, 2.0, and 3.0 Pa for 30 min. And the $MoSe_2$ films were gained by the precursors after the selenization at 500 °C for 10 min.

As shown in Fig. 6, the sample of 0.2 Pa has a friction coefficient of about 0.15 at the beginning of the test. However, the coefficient of friction rises sharply and results in lubrication failure. The average friction coefficient of this sample during the entire test is 0.4310. The $MoSe_2$ film with a sputtering pressure of 1.0 Pa shows a relatively stable lubrication effect during the whole friction test, and the average friction coefficient is calculated as 0.1740. When the power rises to 2.0 Pa, the running-in process of the film is about

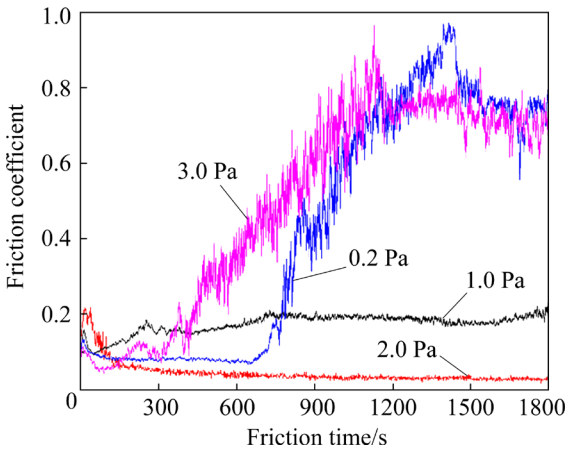

Fig. 6 Friction coefficients of $MoSe_2$ films prepared at different sputtering pressures

150 s, and the average friction coefficient of the entire test reaches the lowest value of 0.0443. Furthermore, the curve of the $MoSe_2$ film prepared at 3.0 Pa changes dramatically during the friction, which has a relatively poor lubrication effect. Generally, when the pressure is 2.0 Pa, the film sample reaches the minimum average friction coefficient and has the best anti-friction performance.

Figure 7 shows the 3D profiles of the wear tracks on the surface of these films. As shown in Figs. 7(a) and (d), the width of the wear scars is larger, reaching about 0.5 and 0.4 mm, respectively. It is supposed that the Ar pressure of sputtering will affect the density of the prepared films, as the dense structure will evolve into a loose and porous structure with the increase in the sputtering pressure [20]. As for the sample of 0.2 Pa, the structure of the film is denser, which is conducive to the initial lubrication stage. However, when the friction time reaches about 700 s in Fig. 6, the film peels off and the GCr15 ball is in direct contact with the steel substrate. The lubrication fails and results in a sharp increase in the friction coefficient. The maximum and average depth of the wear scar are about 5.71 and 2.11 μm, respectively, indicating the peeling off during the friction. In Fig. 7(a), the worn surface is relatively rough without obvious plow grooves, indicating severe plastic deformation. Owing to the rapid failure and peeling of the $MoSe_2$ film, the wear behavior between the GCr15 ball and the substrate is intensified. As shown in Fig. 7(d), when the pressure reaches 3.0 Pa, the $MoSe_2$ film also peels off during the friction, showing a relatively low adhesive strength between the film and substrate. At about 300 s in Fig. 6, the friction coefficient begins to increase and the anti-friction effect of the film begins to drop significantly, which shows obvious adhesion wear. The mean depth of the wear track is about 0.37 μm. As for the film prepared at 1.0 Pa in Fig. 7(b), the depth of the surface wear scar is relatively shallow, which is less than 0.5 μm. While in Fig. 7(c), the sample prepared at 2.0 Pa has the narrowest scar width of about 0.1 mm. The wear rate of the wear track in Fig. 7(c) was calculated as 1.03×10^{-5} $mm^3/(N\cdot m)$.

There are a few plow grooves on surfaces caused by abrasive wear in Fig. 8, including the pitting corrosion caused by fatigue wear. Compared with the lubrication performance of MoS_2 film, which has a friction coefficient of 0.17 and a wear rate of 2.2×10^{-5} $mm^3/(N\cdot m)$ under ambient air reported in the literature [21], the selenized $MoSe_2$ film in Fig. 7(c) shows higher resistance to humid atmosphere and almost half the wear rate.

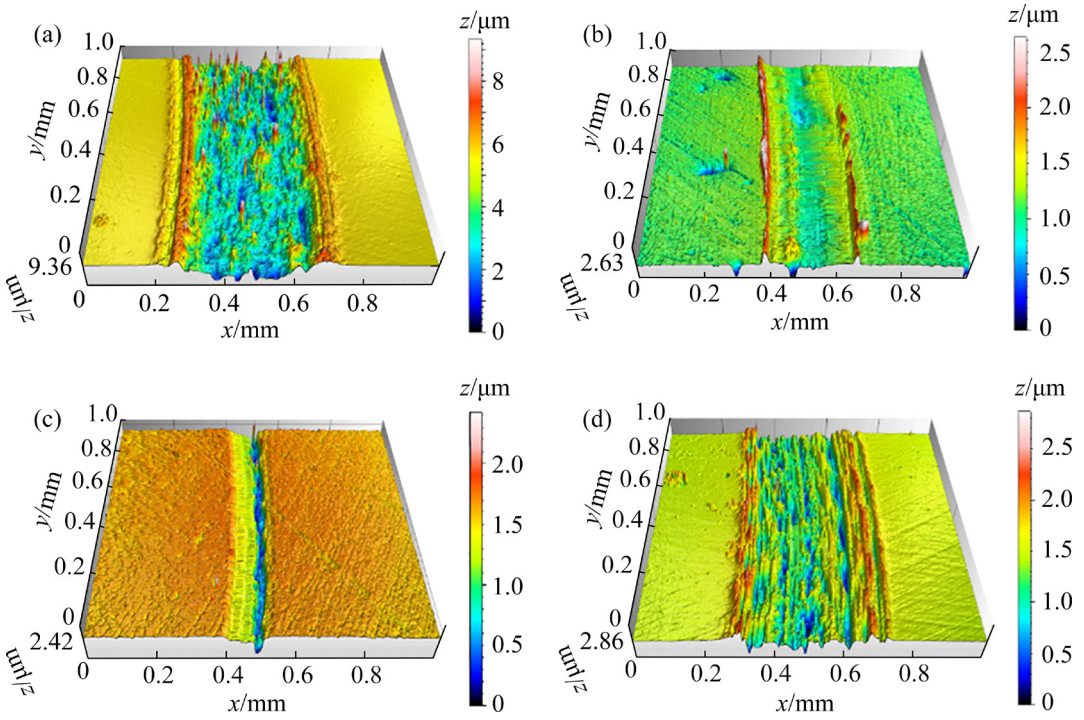

Fig. 7 Surface profiles of wear scars on $MoSe_2$ films prepared at different sputtering pressures: (a) 0.2 Pa; (b) 1.0 Pa; (c) 2.0 Pa; (d) 3.0 Pa

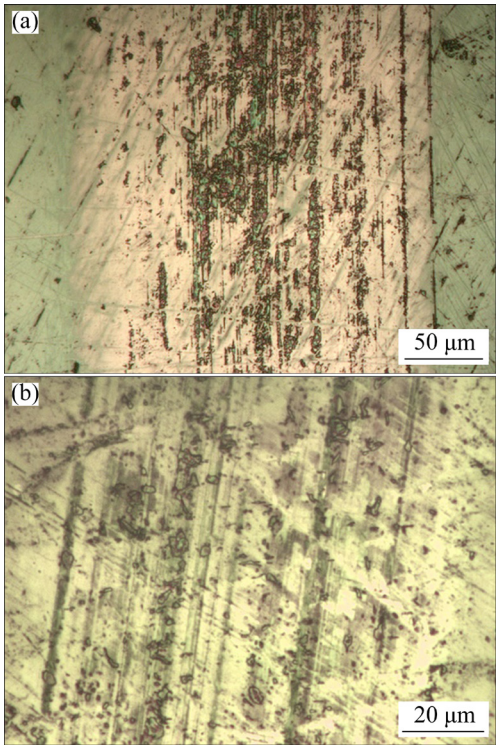

Fig. 8 OM images of wear tracks on $MoSe_2$ films prepared at sputtering pressures of 1.0 Pa (a) and 2.0 Pa (b)

3.2.2 Effect of sputtering time on tribological properties of $MoSe_2$ films

According to the above results, the following experiments were carried out at the sputtering pressure of 2.0 Pa. The $MoSe_x$ precursor films were fabricated at different sputtering time of 10, 20, 30, and 40 min, respectively. And the $MoSe_2$ films were obtained by the $MoSe_x$ precursors after being selenized at 500 °C for 10 min.

Figure 9 shows the friction curves of the $MoSe_2$ films prepared at various sputtering time. When the sputtering pressure is fixed at 2.0 Pa, all films exhibit good lubrication and anti-friction performance. The four samples can all enter the stable wear stage from the running-in stage before 200 s, and the friction curve of the 20 min sample is the first to stabilize after about 100 s in the friction test.

Figure 10 shows the profiles of the wear scars on the films prepared at various sputtering time. As shown in Fig. 10, the widths of wear tracks on surfaces show a slight difference in a range of 0.1−0.15 mm, and there are some plow grooves on the surfaces of these samples, showing the typical abrasive wear.

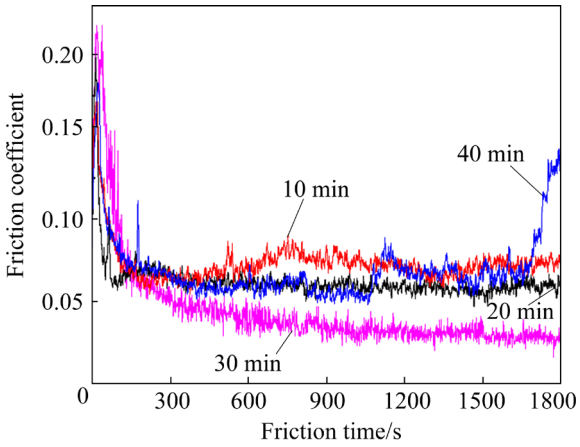

Fig. 9 Friction coefficients of $MoSe_2$ films prepared at different sputtering time

The pitting corrosion caused by fatigue wear can be found in Fig. 11. When the sputtering pressure and power are fixed, the film deposition rate is almost constant, and the thickness of the $MoSe_x$ precursor films deposited onto the surface of the substrates will be adjusted. It is speculated that the thickness of prepared $MoSe_2$ films on stainless substrates will influence the service life of lubrication. By comparing the two samples of sputtering for 30 and 40 min, the mean depth of wear scar in Fig. 10(d) of 0.10 μm is relatively small and the calculated specific wear rate is about 2.54×10^{-6} $mm^3/(N\cdot m)$. The wear rate of this prepared $MoSe_2$ film is lower compared to values reported for $MoSe_2$ (1.4×10^{-5} $mm^3/(N\cdot m)$) in the literature [3].

3.2.3 Effect of selenization temperature on tribological properties of $MoSe_2$ films

According to the results above, the $MoSe_x$ precursor films were prepared at the sputtering pressure of 2.0 Pa for 30 min, and the following selenization research was carried out based on these precursor films. The $MoSe_2$ films were prepared from the precursor films after the selenization at 300, 400, 500, and 600 °C for 10 min. Figure 12 shows the friction curves of these samples. These samples with selenization temperatures of 300 and 500 °C cross from the running-in stage to the stable wear stage rapidly, and the friction curves remain stable. However, when the selenization temperature changes to 400 or 600 °C, the stability of the friction coefficient is relatively low, and there is a sudden increase in these curves. The average friction coefficient reaches the lowest when the selenization temperature is 500 °C.

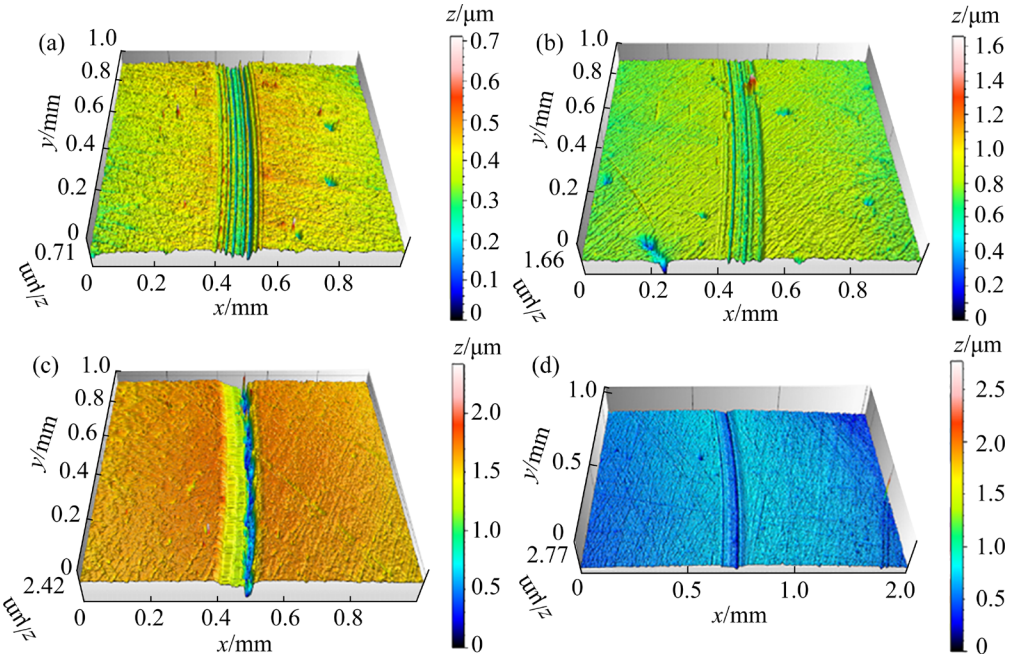

Fig. 10 Surface profiles of wear scars on $MoSe_2$ films prepared at different sputtering time: (a) 10 min; (b) 20 min; (c) 30 min; (d) 40 min

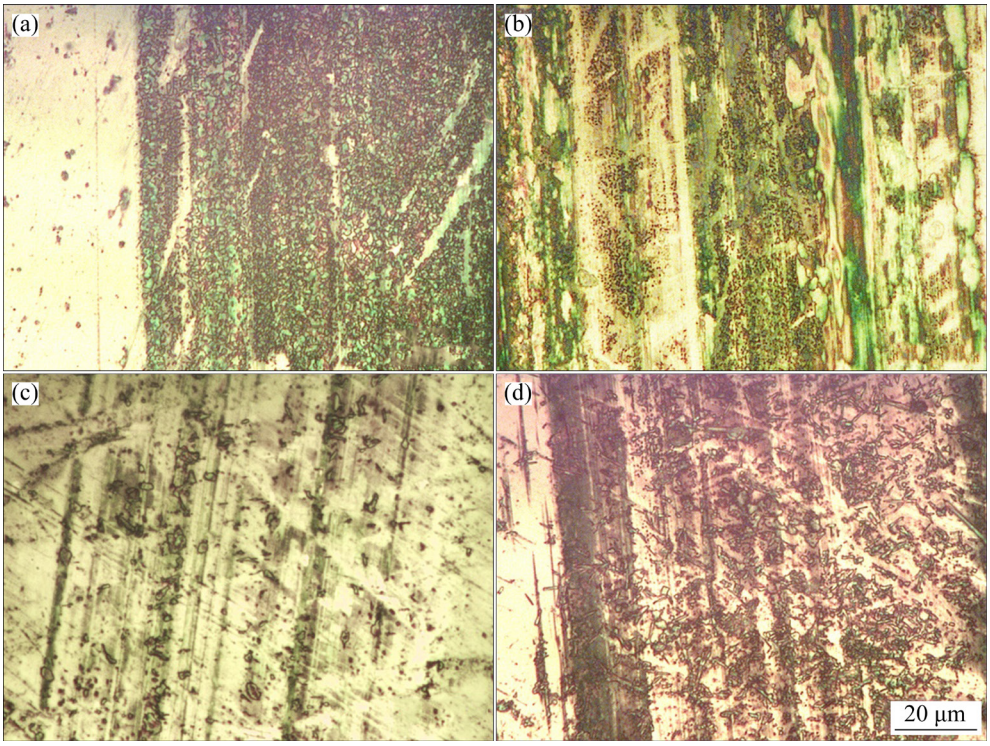

Fig. 11 OM images of wear tracks on $MoSe_2$ films prepared at different sputtering time: (a) 10 min; (b) 20 min; (c) 30 min; (d) 40 min

Figure 13 shows the profiles of the wear scars on the samples prepared at different selenization temperatures after friction tests. The sample with a selenization temperature of 300 °C or 500 °C has a narrow wear width of about 0.1 mm. While the sample prepared at the selenization temperature of 400 or 600 °C has a wear width of over 0.3 mm, showing a serious abrasion. In Figs. 13(c) and (d), the plow grooves on the surfaces are more distinct, showing the typical abrasive wear, while those in

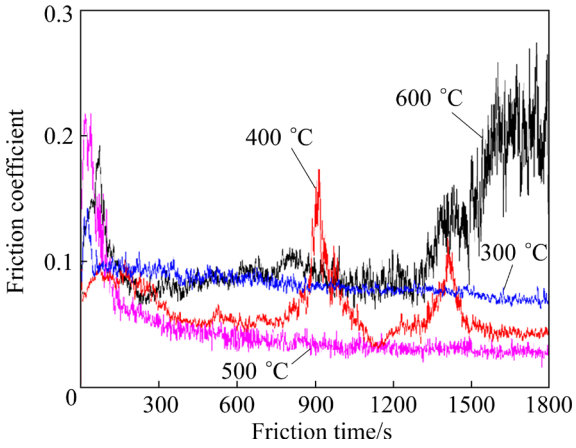

Fig. 12 Friction coefficients of $MoSe_2$ films prepared at different selenization temperatures

Fig. 13(a) show slight abrasive wear, and Fig. 13(b) shows a certain exfoliation, presenting the characteristic of adhesive wear.

Figure 14 shows the optical micrographs of the wear tracks on the $MoSe_2$ films prepared at different selenization temperatures. All films show similar grooves on the wear tracks and varying degrees of adhesive wear, which indicates the formation of adhesion film and wear debris during friction. Obviously, the sample of 500 °C after friction in Fig. 14(c) has a slighter wear track compared with others in Figs. 14(a), (b), and (d). There is more exfoliation caused by adhesive wear visible in Fig. 14(b), which may account for the increase of the 400 °C curve different from the other's curves in Fig. 12. KAUPMEES et al [16] showed that the optimum selenization temperature is about 530 °C, while a higher temperature will result in higher tension and thermal stress which may promote the formation of cracks. This might explain the contraction of stable wear stage in the 600 °C curve shown in Fig. 12.

3.2.4 Effect of selenization time on tribological properties of $MoSe_2$ films

According to the results above, the $MoSe_x$ precursor films were selenized at 500 °C and maintained for 5, 10, 15, and 20 min, respectively, to prepare the $MoSe_2$ films. The influence of selenization time on the tribological performance of the prepared $MoSe_2$ films was investigated.

Figure 15 shows the friction curves of the $MoSe_2$ films prepared at different selenization time during the friction test. When the selenization time is 5 min, the friction coefficient of the $MoSe_2$ film rises rapidly at the beginning of the test, and the average friction coefficient of the entire friction test reaches 0.7269, showing a poor anti-friction effect. When the time is extended to 10 min, the friction curve of the film is relatively stable, and the film enters the stable wear stage after about 150 s, and the friction coefficient shows a slightly decreasing trend. Furthermore, when the precursor film is

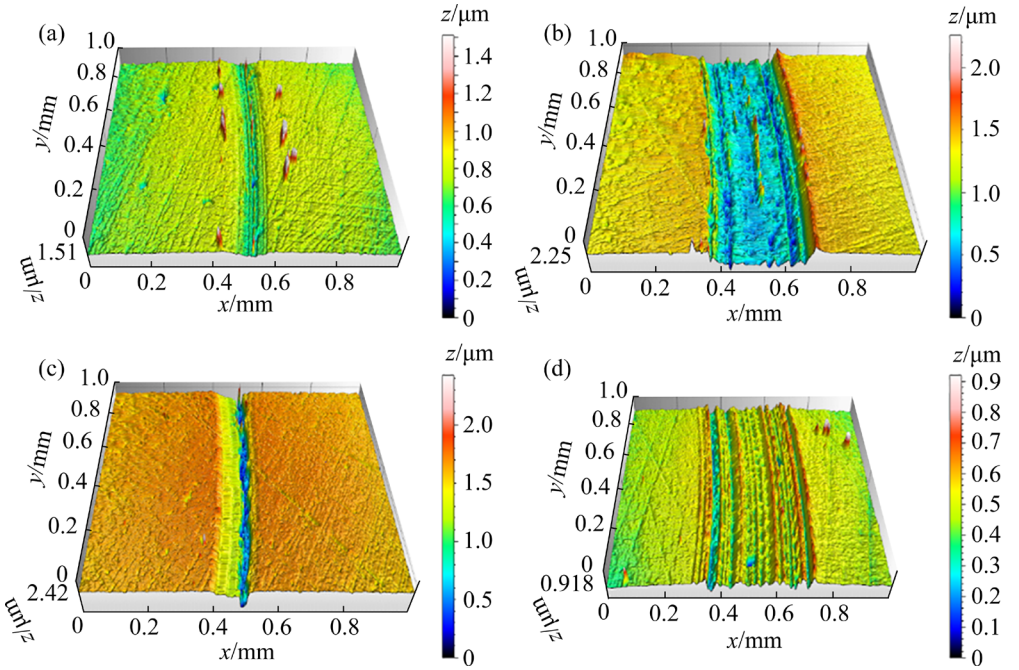

Fig. 13 Surface profiles of wear scars on $MoSe_2$ films prepared at different selenization temperatures: (a) 300 °C; (b) 400 °C; (c) 500 °C; (d) 600 °C

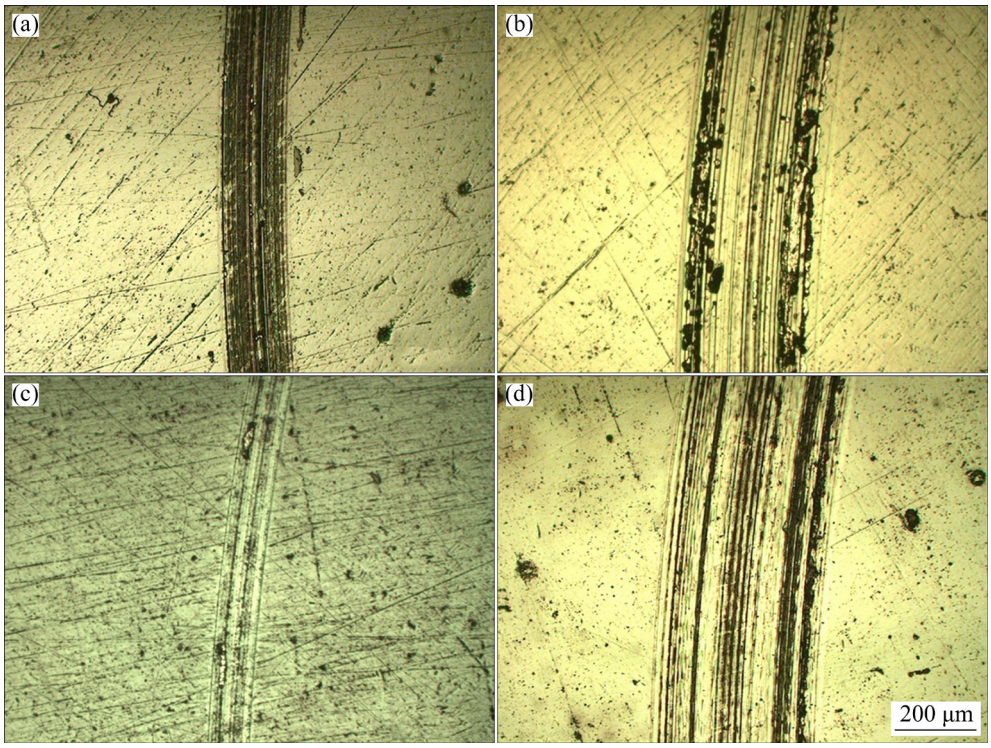

Fig. 14 OM images of wear tracks on $MoSe_2$ films prepared at different selenization temperatures: (a) 300 °C; (b) 400 °C; (c) 500 °C; (d) 600 °C

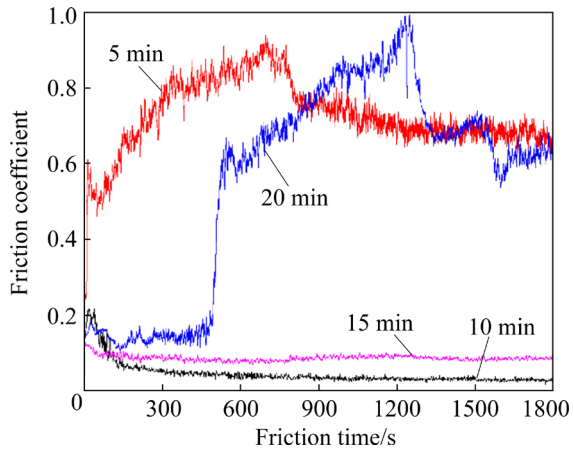

Fig. 15 Friction coefficients of $MoSe_2$ films prepared at different selenization time

selenized for 15 min, the friction coefficient of the sample increases slightly, and it remains stable and shows a good anti-friction effect. However, when the selenization time increases to 20 min, the friction coefficient of the $MoSe_2$ film rises rapidly to about 0.6 at about 500 s.

Figure 16 shows the profiles of the wear scars on $MoSe_2$ films prepared at different selenization time. As shown in Figs. 16(a) and (d), the width of wear scars on the surface exceeds 0.5 mm, showing that the films and substrates are destroyed, and evident peeling off can be noticed in Fig. 16(a). For the samples selenized for 10 and 15 min, the width of the scars is relatively small, as seen in Figs. 16(b) and (c), and these films both have a good anti-friction performance.

In the magnetron sputtering process, the $MoSe_2$ target is mainly sputtered as Mo and Se atoms, and deposited onto the substrate, while the kinetic energies of the atoms are transformed into the energies for particle nucleation, growth, and film formation on the surface of the substrate [14]. Owing to the difference in the sputtering rates between Mo and Se elements, selenium-deficient precursor film was formed, as shown in Fig. 2. Therefore, the non-stoichiometric $MoSe_x$ precursor films were treated by selenization, to promote the reaction between the Se and $MoSe_x$ in the saturated Se vapor atmosphere to form a $MoSe_2$ thin film with a more complete crystal structure. When the selenization time is 5 min, the reaction is inadequate, so the film is incomplete. During the friction test, the incomplete structure may cause severe wear, leading to rapid destruction of the film, as shown in Fig. 16(a). When the selenization time is extended to 10 or 15 min, as shown in Figs. 16(b) and (c), the films react relatively completely, forming

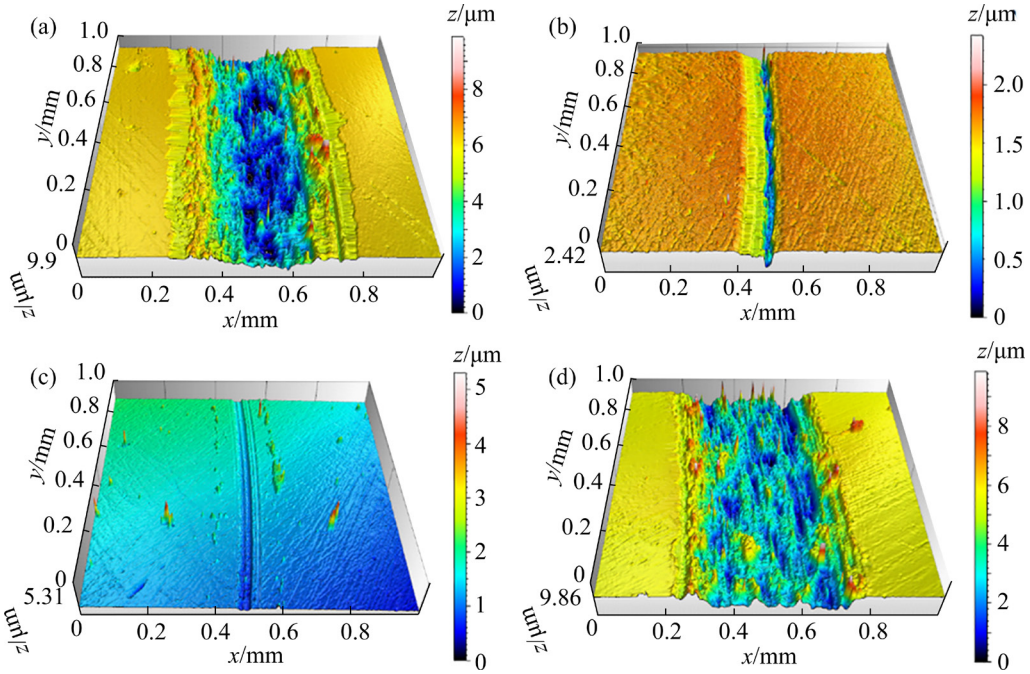

Fig. 16 Surface profiles of wear scars on $MoSe_2$ films prepared at different selenization time: (a) 5 min; (b) 10 min; (c) 15 min; (d) 20 min

an intact $MoSe_2$ protective layer, which reduces the friction coefficient. Furthermore, when the selenization time reaches 20 min, as shown in Fig. 16(d), the excessive treatment may increase the thermal stress in the film, and the film is prone to curling, which reduces the bonding force between the film and the substrate. This sample can maintain a low friction coefficient in the initial stage of the test, but as the friction continues, the $MoSe_2$ film gradually peels off from the substrate, and the GCr15 ball contacts with the substrate directly, resulting in a rapid increase in the friction coefficient and the damage of the film.

3.2.5 Anti-friction mechanism of $MoSe_2$ films

The existence of the $MoSe_2$ film makes the direct friction between the two friction pairs change to the friction between the van der Waals layers of $MoSe_2$. There is no dangling bond between layers, and the weak interlayer forces make it easier to adhere to the metal surface and form a protective layer [5]. There are mainly two possible mechanisms of $MoSe_2$ film to reduce the friction coefficient between friction pairs, and the possible lubrication mechanisms are sketched in Fig. 17.

On the one hand, at the initial stage of the friction test, the GCr15 steel ball touches the surface of the $MoSe_2$ film with a certain pressure. Under the local high stress, local wear appears on the surface of the $MoSe_2$ film. And part of the $MoSe_2$ film will peel off and adhere to the surface of the GCr15 ball, under the existence of shearing force, which is called the adhesion mechanism [22], as shown in Fig. 17(b). Thus, the friction between the steel ball and the film is changed into the friction between the $MoSe_2$ lubrication films. The layered $MoSe_2$ film between the friction pairs will reduce the friction and wear rate, and exhibit a good lubrication effect.

On the other hand, numerous $MoSe_2$ nanosheets and nanoparticles will be formed in the gap between the friction pairs during the friction test, which have a strong diffusion ability. The nanoparticles can provide lubrication by sliding, exfoliation, and rolling [23]. Owing to the constant force of the friction process, these particles can fill the pits, which are embedded between the surface of the friction pair [24], as shown in Fig. 17(c), and achieve the self-repair of the friction surface. This is called the fill in-repair mechanism [25]. In addition, when the $MoSe_2$ nanoparticles and nanosheets between friction pairs are continuously consumed, the friction coefficient of the surface will increase, resulting in an increase in the wear rate. Meanwhile, the increased wear will promote the delamination of $MoSe_2$ film under shearing force and the production of new nanosheets and

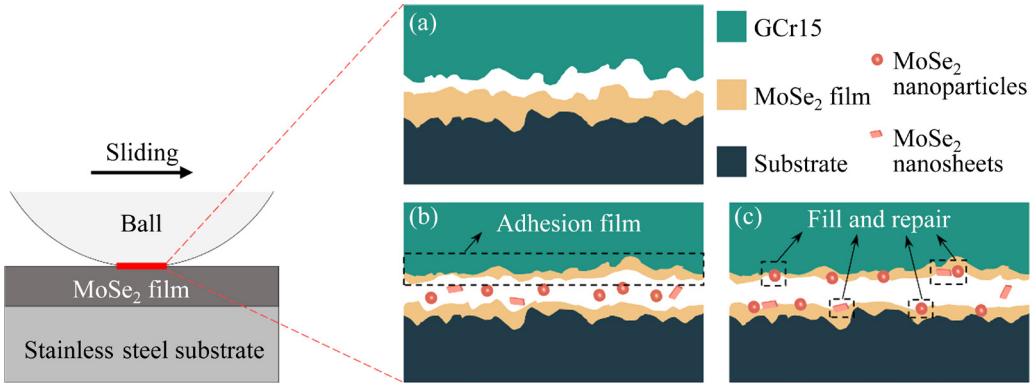

Fig. 17 Schematic diagram of lubrication mechanisms of $MoSe_2$ film on stainless steel substrate during friction test: (a) Before friction; (b) Formation of adhesion layer, $MoSe_2$ nanoparticles and nanosheets during friction; (c) Nanoparticles filling and repairing surface pits

nanoparticles. And this will continuously provide an intact $MoSe_2$ lubricating film on the surface of the friction pairs to reduce the friction and wear rate. Therefore, the $MoSe_2$ film can keep the friction pairs to maintain at a stable and low wear rate.

4 Conclusions

(1) The $MoSe_2$ films were successfully prepared through a two-step method. The prepared $MoSe_2$ films exhibit a preferential orientation with (002) basal plane parallel to the substrate.

(2) The effects of different processing parameters on the tribological performances of prepared films were investigated. The $MoSe_2$ films prepared under low or high sputtering pressure are prone to peeling off during the friction test, and the anti-friction performance is poor. The average friction coefficients of $MoSe_2$ films have little change with the increase of sputtering time. With the increase in selenization temperature, the average friction coefficients of the samples showed a trend of decreasing first and then increasing. In conclusion, the sample sputtered under the argon pressure of 2.0 Pa for 30 min and selenized at 500 °C for 10 min will get the optimized lubrication performance, which can reach the lowest average friction coefficient of 0.0443 and a specific wear rate of 1.03×10^{-5} $mm^3/(N\cdot m)$.

(3) The lubrication mechanisms of the $MoSe_2$ thin-film including the adhesion mechanism and fill in-repair mechanism during the friction process are proposed.

Acknowledgments

The authors are grateful for the financial support from the Natural Science Foundation of Hunan Province, China (No. 2018JJ2524).

References

[1] KIM T I, KIM J, PARK I J, CHO K O, CHOI S Y. Chemically exfoliated 1T-phase transition metal dichalcogenide nanosheets for transparent antibacterial applications [J]. 2D Materials, 2019, 6: 025025.

[2] CHEN Z Y, GUO L L, YAN H X, YAO H H, LI L, LIU Q. Amino functionalization of graphene/graphene-like $MoSe_2$ hybrids as lubricant additives for bismaleimide composites: Preparation, mechanical and tribological properties [J]. Composites Part B: Engineering, 2019, 161: 263−271.

[3] KUBART T, POLCAR T, KOPECKÝ L, NOVÁK R, NOVÁKOVÁ D. Temperature dependence of tribological properties of MoS_2 and $MoSe_2$ coatings [J]. Surface and Coatings Technology, 2005, 193: 230−233.

[4] LAVIK M T, MEDVED T M, MOORE G D. Oxidation characteristics of MoS_2 and other solid lubricants [J]. ASLE Transactions, 1968, 11: 44−55.

[5] LI Y H, LU H L, LIU Q, QIN L G, DONG G N. A facile method to enhance the tribological performances of $MoSe_2$ nanoparticles as oil additives [J]. Tribology International, 2019, 137: 22−29.

[6] WANG X L, GONG Y J, SHI G, CHOW W L, KEYSHAR K, YE G L, VAJTAI R, LOU J, LIU Z, RINGE E, TAY B K, AJAYAN P M. Chemical vapor deposition growth of crystalline monolayer $MoSe_2$ [J]. ACS Nano, 2014, 8: 5125−5131.

[7] HDZ-GARCÍA H M, MUÑOZ-ARROYO R, ALVAREZ-VERA M, BAHRAMI A, MTZ-ENRIQUEZ A I, DÍAZ-GUILLEN J C, HERNÁNDEZ-GARCÍA F A, ACEVEDO-DÁVILA J L, SANTIAGO-BAUTISTA L. Wear resistance of graphenic-nickel composite coating on austenitic stainless steel [J]. Materials Letters, 2020, 281: 128769.

[8] MORÓN R C, RODRÍGUEZ-CASTRO G A, MELO-MÁXIMO D V, OSEGUERA J, BAHRAMI A, MUHL S, ARZATE-VÁZQUEZ I. Multipass and reciprocating microwear study of TiN based films [J]. Surface and

Coatings Technology, 2019, 375: 793−801.
[9] DAZA L G, ACOSTA M, CASTRO-RODRÍGUEZ R, IRIBARREN A. Tuning optical properties of ITO films grown by rf sputtering: Effects of oblique angle deposition and thermal annealing [J]. Transactions of Nonferrous Metals Society of China, 2019, 29: 2566−2576.
[10] SCHARF T W, PRASAD S V, DUGGER M T, KOTULA P G, GOEKE R S, GRUBBS R K. Growth, structure, and tribological behavior of atomic layer-deposited tungsten disulphide solid lubricant coatings with applications to MEMS [J]. Acta Materialia, 2006, 54: 4731−4743.
[11] YAQUB T B, VUCHKOV T, SANGUINO P, POLCAR T, CAVALEIRO A. Comparative study of DC and RF sputtered $MoSe_2$ coatings containing carbon — An approach to optimize stoichiometry, microstructure, crystallinity and hardness [J]. Coatings, 2020, 10: 133.
[12] YAQUB T B, KANNUR K H, VUCHKOV T, PUPIER C, HÉAU C, CAVALEIRO A. Molybdenum diselenide coatings as universal dry lubricants for terrestrial and aerospace applications [J]. Materials Letters, 2020, 275: 128035.
[13] HUDEC T, BONDAREV A, IZAI V, SROBA V, SATRAPINSKYY L, ROCH T, TURINIČOVÁ V, GRANČIČ B, POLCAR T, MIKULA M. Titanium doped $MoSe_2$ coatings—Synthesis, structure, mechanical and tribological properties investigation [J]. Applied Surface Science, 2021, 568: 150990.
[14] LIU Y J, OU C Y, LU C H. Effects of Mo films prepared via different sputtering conditions on the formation of $MoSe_2$ during selenization [J]. Journal of Alloys and Compounds, 2018, 747: 621−628.
[15] MAO X, LI Z Q, ZOU J P, ZHAO G Y, LI D N, SONG Z Q. Growth controlling behavior of vertically aligned $MoSe_2$ film [J]. Applied Surface Science, 2019, 487: 719−725.
[16] KAUPMEES L, ALTOSAAR M, VOLOBUJEVA O, RAADIK T, GROSSBERG M, DANILSON M, MELLIKOV E, BARVINSCHI P. Isothermal and two-temperature zone selenization of Mo layers [J]. Advances in Materials Science and Engineering, 2012, 2012: 345762.
[17] LI H C, GAO D, XIE S L, ZOU J P. Effect of magnetron sputtering parameters and stress state of W film precursors on WSe_2 layer texture by rapid selenization [J]. Scientific Reports, 2016, 6: 36451.
[18] TERRONES H, del CORRO E, FENG S, POUMIROL J M, RHODES D, SMIRNOV D, PRADHAN N R, LIN Z, NGUYEN M A, ELÍAS A L, MALLOUK T E, BALICAS L, PIMENTA M A, TERRONES M. New first order Raman-active modes in few layered transition metal dichalcogenides [J]. Scientific Reports, 2014, 4: 4215.
[19] BOLLERO A, KAUPMEES L, RAADIK T, GROSSBERG M, FERNÁNDEZ S. Thermal stability of sputtered Mo/polyimide films and formation of $MoSe_2$ and MoS_2 layers for application in flexible $Cu(In,Ga)(Se,S)_2$ based solar cells [J]. Thin Solid Films, 2012, 520: 4163−4168.
[20] HUANG Y X, GAO S S, TANG Y, AO J P, YUAN W, LU L S. The multi-functional stack design of a molybdenum back contact prepared by pulsed DC magnetron sputtering [J]. Thin Solid Films, 2016, 616: 820−827.
[21] HUDEC T, ROCH T, GREGOR M, OROVČÍK L, MIKULA M, POLCAR T. Tribological behaviour of Mo−S−N solid lubricant coatings in vacuum, nitrogen gas and elevated temperatures [J]. Surface and Coatings Technology, 2021, 405: 126722.
[22] GUSTAVSSON F, JACOBSON S, CAVALEIRO A, POLCAR T. Frictional behavior of self-adaptive nanostructural Mo−Se−C coatings in different sliding conditions [J]. Wear, 2013, 303: 286−296.
[23] BONDAREV A V, FRAILE A, POLCAR T, SHTANSKY D V. Mechanisms of friction and wear reduction by h-BN nanosheet and spherical W nanoparticle additives to base oil: Experimental study and molecular dynamics simulation [J]. Tribology International, 2020, 151: 106493.
[24] ZHANG W L, CAO Y L, TIAN P Y, GUO F, TIAN Y, ZHENG W, JI X Q, LIU J Q. Soluble, exfoliated two-dimensional nanosheets as excellent aqueous lubricants [J]. ACS Applied Materials & Interfaces, 2016, 8: 32440−32449.
[25] LI W J, HU L F, WANG M Z, TANG H, LI C S, LIANG J Q, JIN Y, LI D S. Synthesis and tribological properties of Mo-doped WSe_2 nanolamellars [J]. Crystal Research and Technology, 2012, 47: 876−881.

两步法制备 $MoSe_2$ 薄膜的结构与摩擦学性能

詹汶峄，邹俭鹏，冒 旭，汤 磊，韦鸿铭

中南大学 粉末冶金国家重点实验室，长沙 410083

摘 要：为了扩大固体润滑剂 $MoSe_2$ 的应用领域，采用两步法制备 $MoSe_2$ 薄膜。首先通过磁控溅射法在基底上沉积 $MoSe_x$ 预制层，随后在 Se 蒸气中进行硒化处理得到 $MoSe_2$ 薄膜。研究溅射和硒化过程对薄膜结构和摩擦学性能的影响。结果表明，两步法所制备的 $MoSe_2$ 薄膜呈(002)晶面平行于基底的择优取向，结晶度得到提高。所制备的 $MoSe_2$ 薄膜在空气环境下具有良好的耐磨性和润滑性能，其最低平均摩擦因数为 0.0443，比磨损率为 1.03×10^{-5} $mm^3/(N\cdot m)$。此外，还探讨了 $MoSe_2$ 薄膜的润滑机理，可通过黏附机制和填充修复机制起到减摩润滑的作用。

关键词：$MoSe_2$ 薄膜；磁控溅射；硒化；摩擦学性能；润滑机制；三维形貌

(Edited by Wei-ping CHEN)